Variation of nonequilibrium processes in the p + Ni system with beam energy

A. Budzanowski,[1] M. Fidelus,[2] D. Filges,[3] F. Goldenbaum,[3] H. Hodde,[4] L. Jarczyk,[2] B. Kamys,[2,*] M. Kistryn,[1] St. Kistryn,[2] St. Kliczewski,[1] A. Kowalczyk,[2] E. Kozik,[1] P. Kulessa,[1,3] H. Machner,[3] A. Magiera,[2] B. Piskor-Ignatowicz,[2,3] K. Pysz,[1,3] Z. Rudy,[2] R. Siudak,[1,3] and M. Wojciechowski[2]
(PISA Collaboration)
[1]*H. Niewodniczański Institute of Nuclear Physics PAN, Radzikowskiego 152, PL-31342 Kraków, Poland*
[2]*M. Smoluchowski Institute of Physics, Jagellonian University, Reymonta 4, PL-30059 Kraków, Poland*
[3]*Institut für Kernphysik, Forschungszentrum Jülich, D-52425 Jülich, Germany*
[4]*Institut für Strahlen- und Kernphysik, Universität Bonn, D-53121 Bonn, Germany*
(Received 8 September 2009; published 13 November 2009)

The energy and angular dependence of double differential cross sections $d^2\sigma/d\Omega dE$ were measured for p, d, t, ^{3,4}He, ^{6,7}Li, ^{7,9}Be, and ^{10,11}B produced in collisions of 0.175 GeV protons with a Ni target. The analysis of measured differential cross sections allowed the extraction of total production cross sections for the ejectiles listed above. The shape of the spectra and angular distributions indicates the presence of other nonequilibrium processes besides the emission of nucleons from the intranuclear cascade and the evaporation of various particles from remnants of intranuclear cascade. These nonequilibrium processes consist of the coalescence of nucleons into light-charged particles during the intranuclear cascade, of the fireball emission, which contributes to the cross sections of protons and deuterons, and of the breakup of the target nucleus, which leads to the emission of intermediate mass fragments. All such processes were found earlier at beam energies 1.2, 1.9, and 2.5 GeV for Ni and Au targets; however, significant differences in the properties of these processes at high and low beam energy are observed in the present study.

DOI: 10.1103/PhysRevC.80.054604 PACS number(s): 25.40.Sc, 25.40.Ve

I. INTRODUCTION

One of the most significant questions to be addressed by studies on proton-nucleus collisions is the predictive power of existing models and computer programs used for their realization. The preceding question is closely related to the two following problems: (i) whether all important physical phenomena are taken into consideration and (ii) whether the parameters of the models are adjusted properly. It is well known that neglect of an important physical phenomenon may be "repaired" in a specific case by appropriate adjustment of free parameters of the model. This procedure cannot, however, be extended to a full set of observables for all targets and energies. Thus a general model must explicitly contain all important physical phenomena.

The traditionally used description of proton-induced reactions at GeV energies assumes that the reactions proceed in two steps. The fast, nonequilibrium step in such a two-step model consists of an intranuclear cascade of nucleon-nucleon collisions with a possible coalescence of the nucleons into complex particles as it is realized, for example, by the INCL4.3 computer program of Boudard *et al.* [1]. This stage of the reaction is assumed to lead to an equilibrated, excited residuum of the target, which, in the following, evaporates particles and/or emits fission fragments. This picture of reactions turned out to be realistic in many situations. It was, however, observed at proton beam energies above several GeV that copious emission of intermediate mass fragments (IMFs), that is, ejectiles heavier than ^{4}He and lighter than fission fragments, appears (cf. [2,3]) as what is interpreted as an analog of the liquid-gas phase transition (cf. [4,5] and references therein). The nucleus, which is treated as a liquid, changes then into a mixture of free nucleons, light-charged particles (LCPs) (particles with $Z \leqslant 2$), and IMFs, treated as a fog. In this case, ejectiles are emitted by only one source: the slowly moving target spectator.

It was recently found, however, that at proton beam energies of 1.2–2.5 GeV, the IMFs and LCPs originating from p + Ni [6] and p + Au collisions [7,8] are emitted from three sources. They are interpreted as a fireball—a fast and hot source consisting of several nucleons—knocked out by the impinging proton and two slower and colder sources, which are believed to be prefragments of the target nucleus appearing because of its breakup, which is caused by strong deformation induced by the fireball emission. The analysis of the experimental data by a traditional model, assuming the presence of intranuclear cascade with the possibility to form complex particles because of coalescence, and evaporation from an equilibrated target remnant could not account for the presence of these sources and could not reproduce the full set of experimental data. On the contrary, the combination of a traditional model with additional inclusion of the emission from the fireball and two other sources, treated within a phenomenological model, led to a perfect description of energy and angular dependencies of all double differential cross sections $d^2\sigma/d\Omega dE$. It is therefore obvious that in a proper theoretical analysis, such phenomena should be taken into consideration.

A question arises about the energy development of the reaction mechanism. It is not clear whether the same picture of the reaction may be applied to other energies below and above the studied proton beam energy range of 1.2–2.5 GeV. In

*ufkamys@cyf-kr.edu.pl

the present study, the investigation of the reaction mechanism of p + Ni collisions is extended to a much lower energy, $E_p = 0.175$ GeV, which is on the border of applicability of the traditional model of an intranuclear cascade followed by evaporation [1,9,10].

To facilitate the comparison of the results from the present study of the reactions in a p + Ni system with results of previous investigations at higher energies in the same nuclear system [6], the present article is organized in a similar way as Ref. [6]. Experimental data are discussed in Sec. II; the theoretical analysis is described in Sec. III, starting from IMF data and followed by the analysis of LCP cross sections; the discussion of results is presented in Sec. IV; and a summary with conclusions is provided in Sec. V.

II. EXPERIMENTAL DATA

The experiment was performed with a self-supporting Ni target of a thickness of about 150 μg/cm^2, irradiated by an internal proton beam of the Cooler Synchrotron of the Jülich Research Center. The experimental setup and data-taking procedure are detailed in Refs. [8] and [11].

Double differential cross sections $d^2\sigma/d\Omega dE$ were measured at seven scattering angles, 16°, 20°, 35°, 50°, 65°, 80°, and 100°, as a function of energy of ejectiles for the following isotopes: ^{1,2,3}H, ^{3,4}He, ^{6,7}Li, ^{7,9}Be, and ^{10,11}B.

The absolute normalization of the cross sections was achieved by comparing the proton differential cross sections measured in the present experiment at 20°, 65°, and 100° with the absolutely normalized proton spectra from the experiment of Förtsch *et al.* [12]. A perfect agreement of the shape of the spectra from both experiments as well as an agreement of their angular dependence can be seen in Fig. 1. It is worthy to point out that the spectra consist of two parts: a low-energy part (energy less than ∼20 MeV)—measured only in the present experiment, where the evaporation of protons from excited target remnants after the intranuclear cascade sets in—and high-energy tails, which are because of preequilibrium processes. In the traditional, two-step model, this part of the spectra comes from the emission of protons from the intranuclear cascade. As will be discussed later, the same two components, representing particles emitted from the equilibrated nuclear system and those from preequilibrium processes, are visible in the spectra of other LCPs and IMFs.

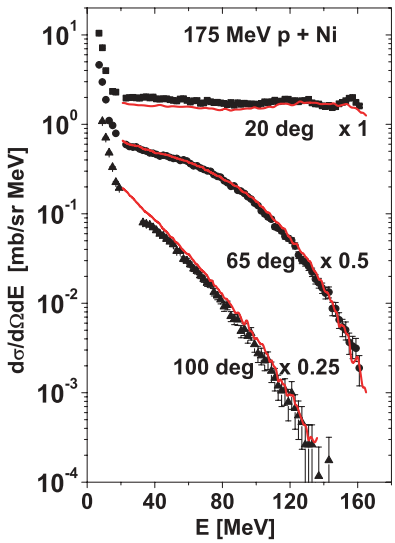

FIG. 1. (Color online) Proton energy spectra measured at 20°, 65°, and 100° in the laboratory system. Lines represent the data from Förtsch *et al.* [12]; symbols depict the data from the present experiment. The spectra were multiplied by factors written in the figure to avoid overlapping the symbols and lines obtained at different angles.

III. THEORETICAL ANALYSIS

The analysis of the present experimental data was performed according to the same procedure as that applied previously to the data from proton-induced reactions on an Ni target at higher energies by Budzanowski *et al.* [6].

The experimental data were first compared with calculations performed in the frame of a two-step model, in which the fast stage was calculated as an intranuclear cascade with the possibility to coalesce the outgoing nucleons into complex LCPs and the slow stage was modeled by evaporation of particles (both LCPs and IMFs) from the excited residuum of the intranuclear cascade, which was assumed to be in equilibrium.

The calculations of the first step of the reaction were done using the INCL4.3 computer program of Boudard *et al.* [1], and the calculations of evaporation of particles were realized by means of the GEM2 computer program of Furihata [13,14]. In both types of calculations, default values of the parameters proposed by the authors were used, and thus no adjustment of the theoretical cross sections to the data was undertaken.

It turned out that the spectra of both LCPs and IMFs were not satisfactorily well reproduced. Therefore a phenomenological analysis was performed, in which the isotropic emission of particles from sources moving in the forward direction (along to the beam) was allowed. Each of the sources had Maxwellian distribution of the energy E available for the two-body decay in which the emission of the detected particles occurred: $d^2\sigma/dEd\Omega \sim \sqrt{E}e^{(-E/T)}$. The velocity of the source $-\beta$ (in units of speed of light), its temperature $-T$ (in MeV), and the contribution to the total production cross section $-\sigma$ (in mb) were treated as free parameters.

Two additional parameters, defining the height B of the Coulomb barrier for emitted particles and the diffuseness d of the transmission function through the barrier, were used with fixed values. Further details of the model are given in the appendix of Ref. [8].

The analysis of IMF data differs from that of LCP cross sections, and thus they are described separately in the following two sections.

A. IMFs

The experimental spectra for ^{6,7}Li, ^{7,9}Be, and ^{11}B measured at 35°, 50°, and 100° scattering angles are shown in Fig. 2 as open circles, together with the theoretical calculations

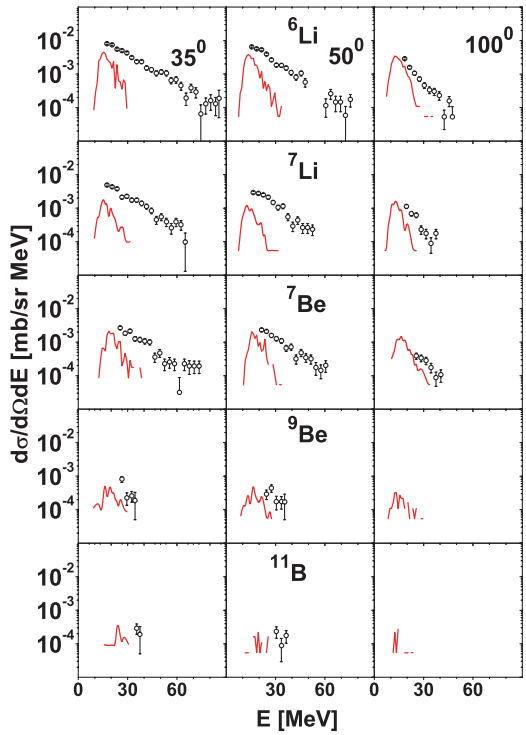

FIG. 2. (Color online) Typical spectra of selected lithium, beryllium, and boron isotopes from p + Ni collisions measured at 35° (left), 50° (middle), and 100° (right) for a 0.175-GeV proton beam impinging onto the Ni target. The detected particles are listed in the central panel of each row. Open circles represent the experimental data, and solid lines correspond to intranuclear cascade followed by evaporation of particles, respectively.

performed in the frame of the two-step model (intranuclear cascade followed by evaporation of particles from the excited remnant of the target nucleus), which are depicted by solid lines. The fluctuations of these lines are because of limited statistics of the model calculations, which were done by the Monte Carlo method and have no physical meaning.

As can be seen, the theoretical spectra are different from the experimental spectra in several ways: (i) the theoretical spectra are almost independent of the scattering angle, whereas the experimental spectra vary with the angle, showing increased slope with a greater scattering angle; (ii) the theoretical spectra are localized at small ejectile energies (smaller than ∼30 MeV), whereas the experimental spectra cover a much larger range of energies, especially for small scattering angles; and (iii) the magnitude of the theoretical cross sections is smaller than the magnitude of the cross sections of the data.

In the second step of the analysis, the emission of IMFs from two moving sources has been calculated, adding the cross sections from both sources. The velocity of the fast source β_2, temperature parameters of both sources T_1 and T_2, and total production cross sections σ_1 and σ_2 from both sources were fitted to obtain the best agreement of the theoretical cross sections with the data for all seven scattering angles simultaneously. The other parameters, that is, velocity of the slow source β_1 and parameters characterizing the Coulomb barrier k_1, k_2 (heights of the Coulomb barrier between ejectile and source in units B, i.e., height of the Coulomb barrier between ejectile and the target nucleus) and $(B/d)_1$, $(B/d)_2$, were fixed. The velocity of the slow source was assumed to be equal to the average velocity of the residual nuclei after the intranuclear cascade $\beta_1 = 0.0036$ as it was extracted from INCL4.3 calculations, and Coulomb barrier parameters were fixed at arbitrarily chosen values k_1= 0.75, $k_2 = 0.3$, and $(B/d)_1 = (B/d)_2 = 5.5$. These parameters do not influence the spectra, with exception of very low ejectile energies; thus the same values of the parameters were taken as those used at higher beam energies [6]. The experimental spectra measured at 35°, 50°, and 100° (open circles) are shown in Fig. 3, together with results of the calculations (lines). The solid line represents the sum of contributions from both sources, the dashed line depicts the cross section originating from the slow source, and the dash-dotted line shows the cross section corresponding to emission from the fast source.

A very good description of the data has been obtained with the parameters varying smoothly from ejectile to ejectile. The values of the parameters are listed in Table I. The errors of the parameters, estimated by a computer program, which searched for best-fit parameters, are also given in the table. Some parameters, closed in square brackets, were fixed during the fit to avoid ambiguity of the parameters, which appears when the data do not put strong enough constraints on the parameters.

As can be seen in Fig. 3, the slow source produces spectra that are almost independent of angle and are similar to those calculated from the two-step microscopic model. The fast source contribution to the spectra is angle-dependent, and

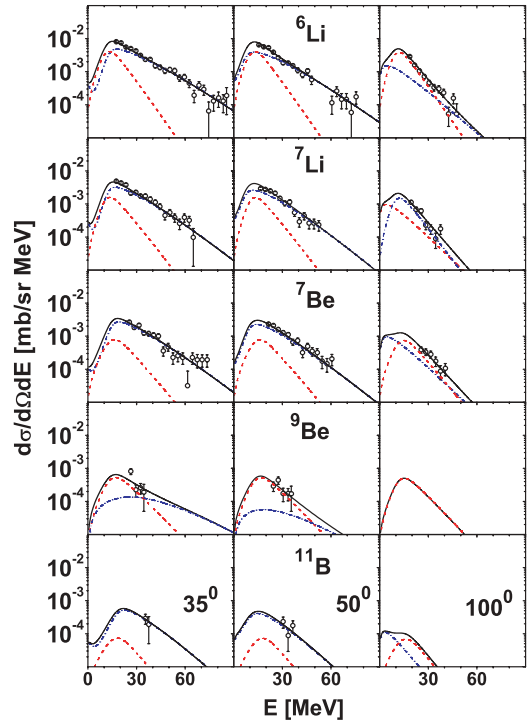

FIG. 3. (Color online) Same as Fig. 2, but dashed, dash-dotted, and solid lines correspond to a slow-emitting source, a fast-emitting source, and the sum of both contributions, respectively.

TABLE I. Parameters of two moving sources for isotopically identified IMFs and for ^{4}He: β_i, T_i, and σ_i correspond to source velocity, its apparent temperature, and the total production cross section, respectively. The sum $\sigma \equiv \sigma_1 + \sigma_2$ is also listed. The left part of the table (parameters with indices 1) corresponds to the slow-moving source, and the right part of the table contains values of parameters for the fast-moving source.

Ejectile	Slow source		Fast source			σ/mb	σ_2/σ	χ^2
	T_1/MeV	σ_1/mb	β_2	T_2/MeV	σ_2/mb			
^{4}He	7.0(3)	39 (3)	0.060(6)	9.7(4)	16.8(2.7)	55.8(4.2)	0.30(6)	32.5
^{6}Li	5.7(4)	0.70(6)	0.045(2)	10.0(2)	0.71(5)	1.41(8)	0.50(5)	1.4
^{7}Li	6.3(8)	0.29(5)	0.041(2)	8.7(4)	0.41(4)	0.70(7)	0.59(8)	1.4
^{7}Be	6.8(1.8)	0.16(7)	0.040(4)	9.0(6)	0.37(6)	0.53(9)	0.70(16)	1.2
^{9}Be	[6.5]	0.12(6)	0.08(2)	[9.0]	0.02(1)	0.14(6)	0.14(7)	1.4
^{10}B	[6.5]	0.10(9)	[0.04]	7.1(3.8)	0.07(4)	0.17(10)	0.42(34)	1.7
^{11}B	[6.5]	0.020(14)	[0.04]	7.0(7.3)	0.06(4)	0.08(5)	0.75(69)	1.3

thus it represents the nonequilibrium process proceeding in the fast stage of the reaction. The spectrum evaluated for this source has a high-energy tail, which allows the reproduction of the high-energy part of the experimental spectra. The relative contribution of this source to the total production cross section is large, as can be seen in Table I [on average, it is equal to 53 (12)%].

B. LCPs

The experimental spectra of LCPs extend to energies higher than 20–30 MeV, which is the upper limit of energy for evaporated particles. Thus it is obvious that the nonequilibrium emission of particles is responsible for the higher-energy part of the spectra. In the case of protons, such nonequilibrium emission appears from the intranuclear cascade before achieving an equilibrium in the target residuum. Coalescence of nucleons of the target with the nucleons escaping from the intranuclear cascade, which may proceed if the relative spatial and momentum positions of nucleons are small enough, has been considered as the process responsible for emission of complex LCPs. Letourneau *et al.* [15] and Boudard *et al.* [1] proposed to treat the coalescence microscopically during the calculation of an intranuclear cascade. Thus this phenomenon is implemented in the INCL4.3 computer program [1], and therefore this program has been applied in the present work for evaluation of intranuclear cascade and coalescence of nucleons, leading to the formation of deuterons, tritons, ^{3}He, and alpha particles. The results of these calculations, coupled with the evaporation of particles evaluated by means of the GEM2 computer program, were compared with the experimental spectra. Very good reproduction of triton and ^{3}He spectra was achieved for all scattering angles, as was significant improvement (in comparison to evaporation spectra alone) of deuteron and α-particle spectra for large scattering angles. However, the small scattering angles of protons, deuterons, and alpha particles were still not satisfactorily well reproduced. Moreover, it was found that the improvement of the description of LCP spectra by inclusion of coalescence deteriorates simultaneously the description of the proton spectra because increases in the production of composite particles occur on account of decreases in the emission of nucleons.

It was thus assumed that an additional process, namely, the emission of a fireball and breakup of the target nucleus, should be taken into consideration as it was found to be necessary for p + Ni and p + Au collisions at higher proton energies (1.2, 1.9, and 2.5 GeV) investigated by the present authors (Refs. [6] and [7], respectively). The parameters of the fireball, that is, its temperature parameter T_3, velocity of the source β_3, and total production cross section associated with this mechanism σ_3, were treated as free parameters and were modified to obtain the best description of experimental cross sections. Other parameters, that is, k_3, the height of the Coulomb barriers in units of B Coulomb barrier between the ejectile and the target nucleus, and B/d, describing diffuseness of the transmission function through the Coulomb barrier, were fixed at arbitrarily assumed values 0.07 and 4.8, respectively. It should be emphasized that the coalescence and evaporation cross sections were allowed to be scaled down by an adjustable factor F—what is physically understood as making room for new nonequilibrium processes, which, in original INCL4.3 + GEM2 calculations, was not considered. Values of the fitted parameters are collected in Table II.

It turns out that inclusion of the emission of LCPs from the fireball into the analysis leads to a very good description of proton and deuteron spectra but gives only negligible modification of triton and ^{3}He theoretical spectra, as is visible in Figs. 4 and 5. The importance of the fireball contribution to proton and deuteron data may be also judged from the ratio of the total production cross section of these particles via fireball emission to the cross section representing the sum of all processes. As can be seen in Table II, the relative fireball contribution to proton and deuteron cross sections is equal to 20 (2)% and 14 (3)%, respectively. This is a rather small value in spite of the fact that it is crucial for a proper description of the spectra, especially at forward angles. On the contrary, the fireball is practically negligible as concerns the total production cross section of tritons and ^{3}He particles. Its contribution is of order 2% only. It should be pointed out that the scaling factor F of INCL4.3 and GEM2 cross sections was fixed for tritons, ^{3}He, and ^{4}He at the same value as for deuterons, that is, $F = 0.8$. Some smaller value will perhaps improve the description of the cross sections because theoretical cross sections of INCL4.3 and GEM2 slightly overestimate the data; however, the contribution of the fireball

TABLE II. Parameters β_3, T_3, and σ_3 correspond to the fireball velocity in units of speed of light, its apparent temperature, and the total production cross section, respectively. Parameter F is the scaling factor of coalescence and evaporation contribution extracted from fits to the proton and deuteron spectra. The numbers in parentheses show fixed values of the parameters. The columns described as $F*\sigma_{INCL}$ and $F*\sigma_{GEM}$ contain total production cross sections because of intranuclear cascade with the coalescence and to evaporation from the target residuum, respectively. The total production cross section obtained by summing all contributions is depicted in the column denoted by σ. In the case of α particles, this column contains also the contribution of emission from slow and fast sources listed in Table I.

Ejectile	β_3	T_3 (MeV)	σ_3 (mb)	F	$F*\sigma_{INCL}$ (mb)	$F*\sigma_{GEM}$ (mb)	σ (mb)	σ_3/σ	χ^2
p	0.232(5)	21.2(1.3)	320(32)	0.83(5)	567	697	1584(32)	0.20(2)	26.8
d	0.240(9)	16.8(2.0)	22.9(3.7)	0.80(3)	104	31	158(5)	0.14(3)	5.3
t	0.142(27)	6.1(4.9)	[0.5]	[0.8]	24.1	2.8	27.4	0.02	14.3
^{3}He	0.205(20)	7.3(3.0)	[0.5]	[0.8]	16.0	4.8	21.3	0.02	18.8
^{4}He				[0.8]	11.5	129	196.3(4.2)		32.5

to triton and ^{3}He spectra is very small, and thus searching F and fireball cross section σ_3 independently led to ambiguities of parameters.

The α-particle cross sections need an additional contribution from two moving sources besides the coalescence and evaporation cross sections. The parameters of these sources are different from fireball parameters but are quite similar to those found earlier for IMFs. It can thus be stated that the α particles behave more as IMFs than as LCPs. The same effect has been observed at beam energies over 1 GeV for the p + Ni system [6].

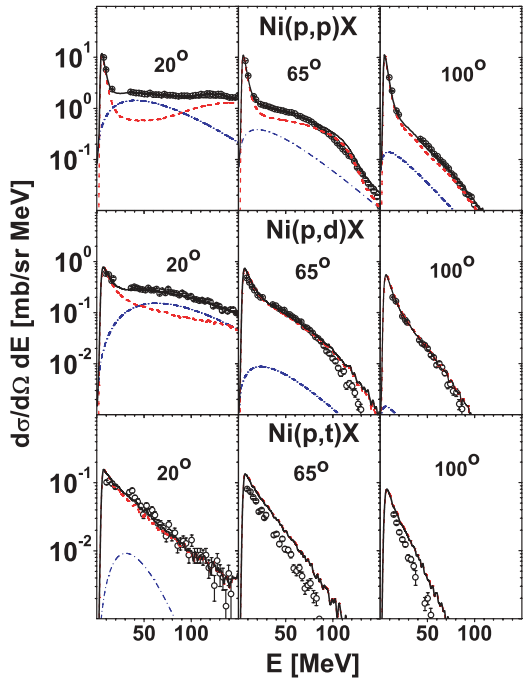

FIG. 4. (Color online) Typical spectra of protons (top), deuterons (middle), and tritons (bottom) measured at 20° (left), 65° (middle), and 100° (right) for a 0.175-GeV proton beam impinging onto the Ni target. Open circles represent the experimental data; dashed, dash-dotted, and solid lines correspond to the two-step model (scaled by factor F; for an explanation, see the text), emission from the fireball, and the sum of both contributions, respectively. Contribution of the fireball is very small for deuterons emitted at large angles and for tritons at all scattering angles.

IV. DISCUSSION

The velocity and temperature parameters of moving sources for all ejectiles are presented in Fig. 6 as a function of the mass of ejectiles. Their values behave in a very similar manner to that observed at higher beam energies in p + Ni [6] and p + Au [7] systems; that is, they belong to three well-separated sets, representing the slow source (β_1 and T_1), the fast source (β_2 and T_2), and the fireball (β_3 and T_3). The ejectile mass dependence may be approximated by a straight line for each source, with a slope that is larger for the fireball than for the fast source. Velocity of the source can be also dependent on the mass of the ejectile because mass of the source may vary for different ejectiles.

As was discussed in a previous article dealing with reactions in the p + Ni system at higher energies [6], the linear

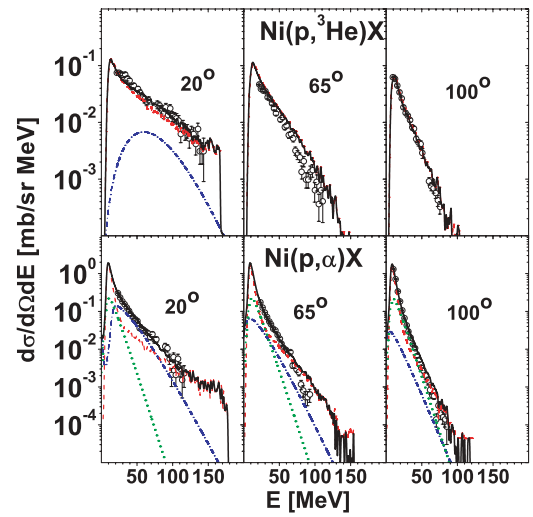

FIG. 5. (Color online) Typical spectra of ^{3}He (top) and ^{4}He (bottom) measured at 20° (left), 65° (middle), and 100° (right) for a 0.175-GeV proton beam impinging onto the Ni target. Open circles represent the experimental data, dashed lines represent results of the two-step model (scaled by factor F), and solid lines depict the sum of all contributions. The dash-dotted line in the upper panel shows the contribution of the fireball, whereas the dash-dotted and dotted lines for ^{4}He denote contributions of fast- and slow-moving sources, respectively.

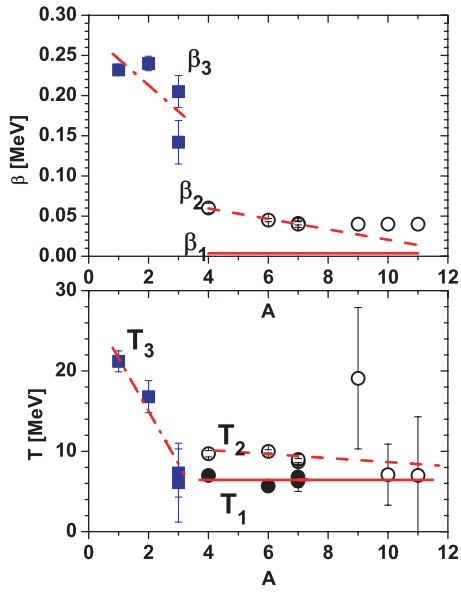

FIG. 6. (Color online) (Bottom) Apparent temperature of the moving sources drawn as a function of the ejectile mass A. Open circles and solid circles represent values of temperature parameters T_2 and T_1 for fast and slow sources, respectively. Solid squares indicate temperature T_3 of the fireball. The solid and dashed lines were fitted to the points representing the lightest IMFs: ^{6}Li, ^{7}Li, ^{7}Be, and ^{4}He. The dash-dotted line was fitted to points representing the LCPs. (Top) Dependence of the velocity of the sources drawn versus the mass of ejectiles. The symbols and lines have the same meaning as for the lower part of the figure, with one exception: The solid circles are not shown because the velocity of the slow source was fixed during the analysis (at velocity $\beta_1 = 0.0036$); it is represented by the solid line in the figure.

dependence of the temperature parameter on the mass of ejectiles can be used for an estimation of mass of the source. The parameters of linear functions describing dependence of the temperature parameter T and velocity β of three sources on the ejectile mass A are collected in Table III. The velocity of the slow source has been fixed at 0.0036 c, that is, at an average velocity of residua of intranuclear cascade extracted from INCL4.3 calculations. The temperature of this source was also found to be independent of the mass of the ejectile and may be represented by its average value, ∼6.5 MeV.

The small and not well defined slope of the mass dependence of the temperature for the fast source and the fireball give very crude estimation of their masses, that is, 45 (33) and 4.2 (1.0) mass units, respectively. The former mass value has too large an error to be used for any further reasoning. The latter value, apart from being not well determined, is smaller than the mass of the fireball extracted from high-energy data, that is, 5.5 (3) mass units [6]. Such a decrease in the mass of the fireball seems to be in accord with the fact that only proton and deuteron spectra have significant contributions of emission from the fireball at 0.175-GeV beam energy, whereas at higher energies, such a contribution was quite large also for tritons and ^{3}He particles.

The next important difference concerns the values of temperature parameters. The temperature parameters at low beam

TABLE III. Temperature and velocity parameters of three sources of ejectiles for the Ni target. In the second column, the parameters obtained in the present study at a beam energy of 0.175 GeV are shown, whereas the third column presents parameters averaged over beam energies 1.2, 1.9, and 2.5 GeV from Ref. [6]. T denotes apparent source temperature (in millions of electronvolts), τ is the temperature parameter corrected for the recoil, A_S represents mass number of the source, and β is its velocity in units of speed of light. The symbol A indicates the mass number of the ejectile. Parameters with index 1, 2, and 3 correspond to a slow source, a fast source, and the fireball, respectively.

Parameter	Ni (0.175 GeV)	Ni (1.2–2.5 GeV)
T_1	6.5(3)	11.2(7)–0.4(2) $*$ A
τ_1	6.5(3)	11.2(7)
A_{S_1}	?	28(15)
β_1	[0.0036]	[0.005]
T_2	11.2(1.0)–0.25(17) $*$ A	22.5(6)–0.8(1) $*$ A
τ_2	11.2(1.0)	22.5(6)
A_{S_2}	45(33)	28(4)
β_2	0.059(5)–0.0034(6) $*$ A	0.044(6)–0.0021(7) $*$ A
T_3	28.1(2.3)–6.6(1.4) $*$ A	52.7(1.1)–9.6(4) $*$ A
τ_3	28.1(2.3)	52.7(1.1)
A_{S_3}	4.2(1.0)	5.5(3)
β_3	0.278(56)–0.033(23) $*$ A	0.209(11)–0.053(5) $*$ A

energy are approximately 2 times smaller than appropriate parameters determined at high energies. This seems to be a natural consequence of the fact that the excitation energy of the target increases with the beam energy because, at approximately the same rate of energy transfer, the total transferred energy must be larger at higher beam energy. The same reasoning can be applied to the increase of the momentum transfer from projectile to the target, which mainly determines the velocity of the target residuum after the intranuclear cascade. According to intranuclear cascade calculations, the velocity of the target residuum at low beam energy, that is, 0.175 GeV, is equal to 0.0036 c, whereas at high energies, it is larger, that is, equal to 0.0050 c, and is almost independent of energy in the range 1.2–2.5 GeV.

The interesting observation, in contradiction with the preceding reasoning, is that the velocities of the fast source as well as of the fireball found from the fit are significantly larger at 0.175-GeV beam energy than at higher beam energies. This may indicate that properties of the reaction mechanism at low energy are different than those at 1.2–2.5 GeV.

According to the present phenomenological model, the sources of ejectiles move along the beam, and thus the momentum conservation requires that the algebraic sum of momenta of all sources should be equal to the projectile momentum ($p_b = 0.60$ GeV/c). Assuming that the fitted values of the fireball velocity β_3 for p, d, t, and ^{3}He are not biased by errors, it is possible to estimate the maximal mass of the fireball—2.7 mass units—which ensures that the momentum of the fireball emitting all these particles is not larger than the beam momentum. Assuming that the mass of the fireball not larger than 3 mass units excludes the possibility of emission of tritons and ^{3}He, what is compatible with the

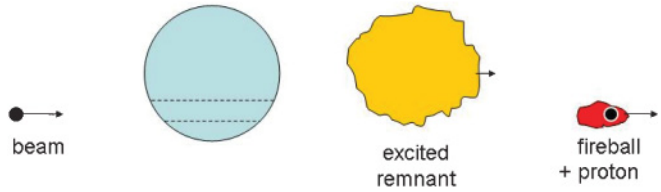

FIG. 7. (Color online) Fireball emission from Ni target at 0.175-GeV beam energy.

fact that contribution of the fireball found from the fit to spectra of these particles is negligibly small. Furthermore, the emission of protons and deuterons is possible from such a three-nucleon fireball, but then their momenta, evaluated with velocities β_3 of Table II, exhaust the full available momentum: $p(\text{fireball}_p) = 0.65$ GeV/c, $p(\text{fireball}_d) = 0.68$ GeV/c. The preceding momenta are even slightly larger than the beam momentum p_b, but given that the fireball velocity was found from unconstraint fit and is biased by errors, the agreement of momenta of the fireballs emitting protons and deuterons with the beam momentum is quite good. Thus the presence of three-nucleon fireball-emitting protons and/or deuterons is in agreement with momentum conservation and shows that full beam momentum is transferred to the fireball. This specifically means that (i) the proton from the beam cannot fly away separately from the fireball and (ii) the creation of a fireball cannot simultaneously lead to breakup of the rest of the target.

The fact that two sources, heavier than the fireball, are observed in the analysis of IMFs means that a breakup of the target occurs. Because the fireball emission cannot be accompanied by the breakup, the breakup must proceed without fireball emission. It is worthy to mention that such a capture of the projectile leading to excitation of the nucleus without emission of the fireball has been discussed by Aichelin *et al.* [16]. They estimated that protons of energies smaller than 0.2–0.25 GeV should be captured without sending the fireball. The excited nucleus created during such a process may deexcite by emission of particles, in a similar way to the heavy residuum of the intranuclear cascade, but may also break up, which leads to the emission of two excited sources of particles, as in our picture of the reaction mechanism.

The fireball emission and the breakup of the target, illustrated by Figs. 7 and 8, may appear at low energy, for example, 0.175 GeV, only exclusively. It is important to emphasize that nevertheless, both are observed in the analyzed

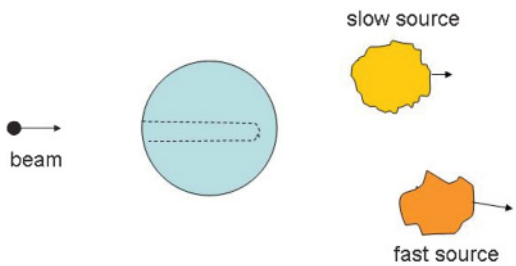

FIG. 8. (Color online) Breakup of Ni target at 0.175-GeV beam energy.

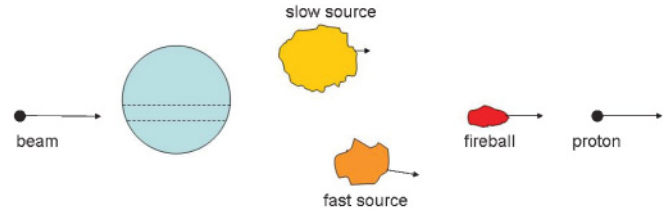

FIG. 9. (Color online) Fireball emission from Ni target at high beam energy (over 1 GeV).

data. This may be connected with the fact that at different impact parameters, the straight path of the proton through the target has a different length. The peripheral collisions correspond to shorter paths through the nucleus, that is, to a smaller stopping power, whereas the central collisions, on the contrary, correspond to the longest paths and the strongest stopping power. The estimation of Aichelin *et al.* [16] should thus be treated as a specific case for central collisions.

The proton impinging with high kinetic energy, for example, 1.2 GeV or higher, can move through the nucleus, knocking out a fireball, but the relative momentum of the proton and the fireball may be so large that the proton flies independently of the fireball. Then the momentum of the fireball is smaller than the momentum of the beam and is not related to the beam momentum in an unambiguous manner. This may be a reason why the velocity of the fireball, observed in $p+$ Ni collisions in the proton energy range from 1.2 to 2.5 GeV [6], is smaller than that observed at 0.175 GeV. Moreover, it does not change significantly, in contrast to strong variation of the beam energy.

A schematic of this reaction mechanism is shown in Fig. 9 for p + Ni collisions at energies above ∼1 GeV.

V. SUMMARY AND CONCLUSIONS

The double differential cross sections $d^2\sigma/d\Omega dE$ for the production of ^{1,2,3}H, ^{3,4}He, and light IMFs (^{6,7}Li, ^{7,9}Be, ^{10,11}B) in collisions of protons with a Ni target have been measured at 0.175-GeV beam energy. The aim of the study was to investigate whether the nonequilibrium processes, which were found to play an important role at higher energies (1.2, 1.9, and 2.5 GeV) [6], are also present at such low energy as 0.175 GeV.

The data were analyzed using a two-step microscopic model. The first step of the reaction was described as the intranuclear cascade of nucleon-nucleon collisions initiated by the proton from the beam. It was allowed that during the intranuclear cascade, the coalescence of nucleons into complex LCPs may proceed. An emission of nucleons from the cascade as well as an emission of LCPs created because of the coalescence were the only nonequilibrium processes taken explicitly into consideration by this model. The second step of the reaction was assumed to be an evaporation of particles (nucleons, LCPs, and IMFs) from the equilibrated target residuum after the intranuclear cascade. It was found that the main properties of the spectra of LCPs are well reproduced by the model, with the exception of forward-scattering angles

in proton and deuteron channels and all angles in the alpha particle channel. The IMF spectra were also not satisfactorily reproduced, especially for high-energy IMFs.

It is worthy to point out that a good-quality description of triton and ^{3}He spectra by coalescence of nucleons and evaporation was achieved with the INCL4.3 and GEM2 computer programs, which used default values of the parameters. Such a good agreement of theoretical cross sections with the data measured at 0.175-GeV beam energy is astonishing because, according to the authors of the computer programs [1,10], the present beam energy is on the border of the energy range at which the concept of intranuclear cascade is applicable.

A phenomenological analysis was performed, assuming that additional processes appear, which may be simulated by the emission from three moving sources, as was successfully done at higher energies. It was found that the cross sections of proton and deuteron emission can be very well described when emission from a fireball, that is, a fast and hot source moving in the forward direction, was taken into account. The contribution of this process to the total production cross sections is rather small—20% for protons and 14% for deuterons—however, it significantly improves the description of the spectra at forward angles. Good reproduction of triton and ^{3}He spectra by a two-step process, in which the coalescence of nucleons was very important, did not need any significant contribution of other nonequilibrium processes. The description of alpha particle spectra and IMF spectra was much improved by inclusion of emission from two moving sources, which were interpreted as prefragments of the target nucleus created because of breakup of this nucleus caused by an impinging proton.

Because of a very good description of energy and angular dependencies of differential cross sections $d^2\sigma/d\Omega dE$, it was possible to extract total production cross sections for all investigated ejectiles. These cross sections are listed in Tables I and II for IMFs and LCPs, respectively.

The preceding picture of the reaction mechanism agrees generally with the picture of the nonequilibrium reactions investigated at higher beam energies. However, there specific properties of the nonequilibrium reactions were found, appearing at 0.175 GeV but not at high energies: (i) The fireball exhausts the total available momentum, and thus it cannot be accompanied by breakup of the target remnant, and (ii) the breakup of the target appears because of capture of the proton without emission of the fireball.

ACKNOWLEDGMENTS

The technical support of A. Heczko, W. Migdał, and N. Paul in preparation of the experimental apparatus is greatly appreciated. This work was supported by the European Commission through European Community-Research Infrastructure Activity under the FP6 "Structuring the European Research Area" program (Hadron Physics, Contract No. RII3-CT-2004-506078, and FP6 IP-EUROTRANS FI6W-CT-2004-516520). M.F. appreciates financial support of the Polish Ministry of Science and Higher Education (Grant No. N N202 174735, Contract No. 1747/B/H03/2008/35). This work was also partially supported by the Helmholtz Association through funds provided to the virtual institute "Spin and Strong QCD" (Grant No. VH-VI-231).

[1] A. Boudard, J. Cugnon, S. Leray, and C. Volant, Nucl. Phys. **A740**, 195 (2004).
[2] J. Richert and P. Wagner, Phys. Rep. **350**, 1 (2001).
[3] V. E. Viola *et al.*, Phys. Rep. **434**, 1 (2006).
[4] V. A. Karnaukhov *et al.*, Phys. Rev. C **67**, 011601(R) (2003).
[5] V. A. Karnaukhov *et al.*, Phys. Rev. C **70**, 041601(R) (2004).
[6] A. Budzanowski *et al.*, arXiv:0908.4487 [nucl-ex] (to be published).
[7] A. Budzanowski *et al.*, Phys. Rev. C **78**, 024603 (2008).
[8] A. Bubak *et al.*, Phys. Rev. C **76**, 014618 (2007).
[9] J. Cugnon, Nucl. Phys. **A462**, 751 (1987).
[10] J. Cugnon, C. Volant, and S. Vuillier, Nucl. Phys. **A620**, 475 (1997).
[11] R. Barna *et al.*, Nucl. Instrum. Methods Phys. Res. A **519**, 610 (2004).
[12] S. V. Förtsch, A. A. Cowley, J. J. Lawrie, D. M. Whittal, J. V. Pilcher, and F. D. Smit, Phys. Rev. C **43**, 691 (1991).
[13] S. Furihata, Nucl. Instrum. Methods Phys. Res. B **171**, 251 (2000).
[14] S. Furihata and T. Nakamura, J. Nucl. Sci. Technol. Suppl. **2**, 758 (2002).
[15] A. Letourneau *et al.*, Nucl. Phys. **A712**, 133 (2002).
[16] J. Aichelin, J. Hüfner, and R. Ibarra, Phys. Rev. C **30**, 107 (1984).